

Absorption Lineshapes in Two-Dimensional Electron Spin Resonance and the Effects of Slow Motions in Complex Fluids

SUNIL SAXENA AND JACK H. FREED

Baker Laboratory of Chemistry, Cornell University, Ithaca, New York 14853-1301

Received October 18, 1996

A methodology for obtaining pure absorption two-dimensional electron spin resonance spectra is presented for the case of large inhomogeneous broadening and/or slow motions. For slow motions, the spectra consist of “complex Lorentzians” superimposed with complex weighting factors, presenting a challenge to obtaining absorption spectra. It is shown how absorption-type spectra can be recovered for the two-pulse COSY and SECSY experiments in such cases. For three-pulse 2D ELDOR experiments, absorption lineshapes can be obtained for the autopeaks, whereas the cross peaks would be of mixed-mode character, in general. However, for practical cases the dispersive components in the cross peaks will be relatively small. Theoretical and experimental absorption spectra are provided to illustrate the method and to show the improved resolution obtained from absorption lineshapes. In particular, the variation in linewidths across a SECSY spectrum, which is a key component in elucidating motional dynamics, is clearly rendered in the pure absorption mode. A convenient method for introducing the necessary phase corrections for the slow-motional spectra is also provided. © 1997 Academic Press

INTRODUCTION

Recent advances in digital electronics and microwave technology have opened up the field of two-dimensional electron spin resonance (1, 2). At the same time, the development of a comprehensive theory for 2D ESR (3) based on the stochastic Liouville equation (4) has enabled the rigorous analysis of slow-motional and inhomogeneously broadened 2D ESR spectra from complex fluids (5, 6). The 2D ESR lineshapes in complex fluids are crucial to obtaining reliable motional and ordering parameters.

While the collection of the signal is performed in a phase-sensitive and dual-quadrature fashion, the analysis of the slow-motional spectra has typically been restricted to the magnitude domain because of the inapplicability of standard methods used to extract the pure absorption signals from fast-motional 2D ESR spectra with little inhomogeneous broadening (1). This inevitably leads to a loss of resolution because of the contributions of the broad dispersion peaks, as is well documented in NMR (7–9). Linewidths in the

absorption spectrum are narrower than those in the magnitude spectrum. For Lorentzian lines, the peak widths at half-height are $\approx T_2^{-1}$ compared to $3^{1/2}T_2^{-1}$ for the magnitude spectrum. In the wings of the spectrum this resolution enhancement is even more dramatic because the dispersive parts of Lorentzian peaks decay more slowly, as $(\omega - \omega_0)^{-1}$. Thus adjacent resonant lines will experience more overlap, including the appearance of apparent, but not real, cross peaks. Also, noise in the pure-phase spectrum is randomly distributed (i.e., equal positive and negative components) while it appears as positive definite in the magnitude spectrum. In addition, the mixture of absorption and dispersion can lead to the problem of “phase twist” of spectral lines (8).

Earlier work using swept-field 2D ESE demonstrated (10, 11) that the spectra in the slow-motional regime were very sensitive to T_2 variations across the spectrum. This was found to be particularly important for determining the details of the motional mechanism (e.g., whether the molecule rotates by jump, free diffusion, or Brownian diffusion).

The natural candidate to monitor this T_2 variation in 2D FTESR is the SECSY experiment. However, in this experiment, finite pulses and dead times lead to a phase variation across the spectrum. This causes a mixture of absorption and dispersion in both frequency domains, which itself leads to a loss in resolution because of interference from the broad dispersive components. Either one makes the necessary corrections (by methods we discuss below), or else for convenience magnitude spectra may be studied, wherein the phase corrections are unnecessary, but the resolution is reduced. As a result, the variation of linewidths across the spectrum is rarely apparent in the magnitude displays, so it is crucial to obtain pure absorption lineshapes. This problem is exacerbated in the near rigid limit where the resonance frequencies of the “dynamic spin packets” are virtually a continuum.

A number of methods have been developed for obtaining absorption spectra in high-resolution 2D NMR (12, 13) and in echo-detected NMR (14, 15). In 2D ESR, absorption spectra can be readily obtained in the fast-motional regime using linear predictive methods (LPSVD), when there is

little inhomogeneous broadening (16). It should be pointed out that the NMR methods of Keeler and Neuhaus (13) are strictly valid only for negligible inhomogeneous broadening. This is discussed in the Method section after formulating the problem in the context of slow-motional theory.

The more challenging case of slow motions in magnetic resonance (where the spectra are very sensitive to details of the motional dynamics) requires more care as the spectrum consists of a sum of complex Lorentzians coupled by *complex* weighting factors (3, 10, 11, 17, 18). Methods used so far in NMR (14, 15) are based on the simplifying assumptions that these weighting factors are real. This is discussed in more detail in the Method section. Furthermore, the LPSVD method is unsatisfactory since it approximates the very complicated lineshapes by a sum of decaying sinusoids, which have little relation to the fundamental dynamic modes [or dynamic spin packets; cf. (2)] predicted by theory. Hence the problem of obtaining absorption lineshapes has so far remained unresolved in both 2D ESR and 2D NMR (19). In the Method section we propose a procedure for obtaining absorption spectra for the two-pulse COSY and SECSY experiments. The method is extended to the 2D ELDOR case and the limitations of this approach are pointed out. It is shown how experimental spectra may be conveniently phase corrected. Finally, experimental and theoretical examples are provided under Results and Discussion.

METHOD

Formulation of the Problem

The main classes of 2D ESR experiments discussed are the two-pulse COSY and SECSY and the three-pulse 2D ELDOR (a 2D exchange experiment). The pulse sequences are shown in Fig. 1. In the two-pulse experiments, the first pulse creates transverse magnetization (i.e., ± 1 coherences) which evolves for a period t_1 . The signal is measured during t_2 for a range of settings of t_1 . In the SECSY experiment, inhomogeneous broadening is refocused along t_1 , and hence the technique provides the homogeneous linewidths (i.e., intrinsic T_2 's) across the spectrum, along ω_1 (2).

In the three-pulse experiment, the first pulse again nutates the spins into the x - y plane (providing ± 1 coherences), following which they are "frequency labeled" during the evolution period t_1 . A second pulse converts this magnetization into the z direction, (i.e., zero-order coherences) where it exists for a time T (the mixing time), during which the spins can be exchanged to different resonant frequencies leading to a magnetization transfer. Hence, after the third pulse, cross peaks can appear due to spins that precessed at $\omega_1 = \omega_a$ during t_1 and $\omega_2 = \omega_b$ during t_2 . The principal mechanisms for magnetization transfer are the electron-nuclear dipolar (END) and Heisenberg exchange (ω_{HE}) inter-

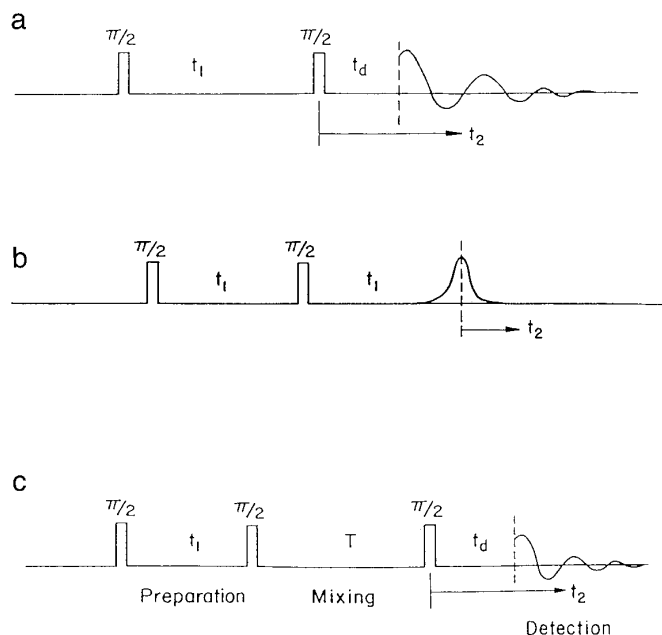


FIG. 1. Basic pulse sequences in 2D ESR. (a) COSY, (b) SECSY, and (c) 2D FT ELDOR.

actions (1, 2). In the very slow-motional regime another mechanism becomes relevant. Here each point in ω_2 refers to an orientation or a set of orientations of the molecule with respect to the dc magnetic field. Cross peaks can develop due to the "real time" reorientation of the molecule during the mixing time. Since the orientations provide a continuum, this "motional" cross-peak development results in an apparent broadening of the autopeaks (3).

The quantitative analysis of slow-motional spectra relies on theoretical simulations based on the stochastic Liouville equation (SLE) (3, 4, 20, 21). The dual-quadrature 2D ESR signal will, in general, provide two types of coherence signals, the S_{c-} (the "echo-like" or the N type) and the S_{c+} (the "FID-like" or the P type), which are then fit to theory. For slow-motional 2D FT spectral calculations, it is necessary to diagonalize the stochastic Liouville superoperator, designated here by \mathbf{L} , in each of the diagonal (zero-order coherence) and off-diagonal (± 1 order coherence) subspaces, i.e.,

$$\mathbf{O}_1^\dagger \mathbf{L}_1 \mathbf{O}_1 = \Lambda_1, \quad \mathbf{O}_0^\dagger \mathbf{L}_0 \mathbf{O}_0 = \Lambda_0, \quad \mathbf{O}_{-1}^\dagger \mathbf{L}_{-1} \mathbf{O}_{-1} = \Lambda_{-1}. \quad [1]$$

Here the subscripts 0, ± 1 refer to the order of the coherence, while \mathbf{O} and Λ are the complex eigenvectors and eigenvalues of the stochastic Liouville operator, \mathbf{L} . The real parts of $\Lambda_{\pm 1}$ provide the homogeneous linewidths (i.e., T_2^{-1}) and the

imaginary parts are the resonant frequencies of the ‘‘normal modes’’ or ‘‘dynamic spin packets.’’

Detailed expressions for \mathbf{L} are given elsewhere (3). A detailed discussion of the properties of \mathbf{O} and Λ is provided in Ref. (22). The relevant results are reproduced here. For fast motions (i.e., the motional narrowing limit), the eigenvectors are pure real and the eigenvalues in the diagonal space are pure real, providing simply the electron and nuclear spin flip rates and the cross-relaxation rates. For slow motions \mathbf{O} and Λ become complex, in general. However, in the diagonal subspace, the eigenvalues Λ_0 are either pure real or come in complex conjugate pairs with eigenvectors such that the combination can be written as real oscillating sinusoids.

For the two-pulse COSY experiment, the $S_{c\pm}$ terms (corresponding to the coherence pathways $0 \rightarrow \mp 1 \rightarrow -1$) are given by (3)

$$S_{c\pm}(t_1, t_2) = \sum_{l,n,j} C_{ln} B_{lj}^{\pm} \exp[-(\Lambda_{\mp 1})_j t_1] \times \exp[-(\Lambda_{-1})_n t_2] \exp[-\Delta(t_2 \pm t_1)^2] \quad [2]$$

$$C_{ln} = \sum_p (\nu_{-1})_p (\mathbf{O}_{-1})_{pn} (\mathbf{O}_{-1})_{ln} \quad [3]$$

$$B_{lj}^{\pm} = \sum_t (\mathbf{O}_{\mp 1})_{lj} (\mathbf{O}_{\mp 1})_{tj} (\nu_{\mp 1})_t, \quad [4]$$

where $\nu_{\pm 1}$ represents the two counterrotating transition moment vectors that specify the transverse magnetization created by the first pulse, and $\Delta = 2\pi^2 \Delta_g^2$. Δ_g represents the additional inhomogeneous broadening, assumed to be Gaussian.

The 2D ELDOR signal (corresponding to the coherence pathway $0 \rightarrow \mp 1 \rightarrow 0 \rightarrow -1$) is given by a similar expression:

$$S_{c\pm}(t_1, T, t_2) = \sum_{l,n,m,j} C_{lnm} B_{lj}^{\pm} \exp[-(\Lambda_{\mp 1})_j t_1] \times \exp[-(\Lambda_0)_m T] \exp[-(\Lambda_{-1})_n t_2] \times \exp[-\Delta(t_2 \pm t_1)^2] \quad [5]$$

$$C_{lnm} = \sum_{p,k} (\nu_{-1})_p (\mathbf{O}_{-1})_{pn} (\mathbf{O}_{-1})_{kn} (\mathbf{O}_0)_{km} (\mathbf{O}_0)_{lm} \quad [6]$$

$$B_{lj}^{\pm} = \sum_t (\mathbf{O}_{\mp 1})_{lj} (\mathbf{O}_{\mp 1})_{tj} (\nu_{\mp 1})_t. \quad [7]$$

Note that Λ_0 is real and B and C are complex, in general. In the absence of nuclear modulation, the eigenvalues and eigenvectors of the two off-diagonal spaces are complex conjugates of each other (i.e., $\mathbf{O}_{-1} = \mathbf{O}_1^*$ and $\Lambda_{-1} = \Lambda_1^*$; therefore $B_{lj}^{-1} = B_{lj}^{1*}$).

Experimentally, one measures a mixture of both S_{c-} and S_{c+} . Quadrature detection in t_2 gives phase discrimination

in ω_2 . We collect two signals S' and S'' for the 2D ELDOR given by

$$S'(t_1, T, t_2) = \frac{1}{2} \sum_{lmn} C_{lmn} \exp[-(\Lambda_0)_m T] \times \exp[-(\Lambda_{-1})_n(t_2 + b_2) - ia_2] \times \sum_j [\exp\{-[\Delta(t_2 + t_1)^2]\} \times B_{lj}^+ \exp\{-(\Lambda_{-1})_j(t_1 + b_1)\} + \exp\{-[\Delta(t_2 - t_1)^2]\} \times B_{lj}^- \exp\{-(\Lambda_{+1})_j(t_1 + b_1)\}] \quad [8]$$

$$S''(t_1, T, t_2) = \frac{1}{2i} \sum_{lmn} C_{lmn} \exp[-(\Lambda_0)_m T] \times \exp[-(\Lambda_{-1})_n(t_2 + b_2) - ia_2] \times \sum_j [\exp\{-[\Delta(t_2 + t_1)^2]\} \times B_{lj}^+ \exp\{-(\Lambda_{-1})_j(t_1 + b_1)\} - \exp\{-[\Delta(t_2 - t_1)^2]\} \times B_{lj}^- \exp\{-(\Lambda_{+1})_j(t_1 + b_1)\}]. \quad [9]$$

Analogous equations for the COSY/SECSY can be written. Phase distortions due to imperfect pulses and finite dead times (cf. below) are included by the terms a_2 , b_1 , and b_2 . The signals from the two coherence pathways are given by the simple linear combination (23)

$$S_{c\pm}(t_1, T, t_2) = S'(t_1, T, t_2) \pm i \times S''(t_1, T, t_2). \quad [10]$$

In the absence of inhomogeneous broadening, the collected signal reduces to (I)

$$S'(t_1, T, t_2) = \sum_{l,n,m} C_{lnm} \exp[-(\Lambda_0)_m T] \times \exp[-(\Lambda_{-1})_n(t_2 + b_2) - ia_2] \times \Re \sum_j B_{lj} \exp[-(\Lambda_j)(t_1 + b_1)] \quad [11]$$

$$S''(t_1, T, t_2) = \sum_{l,n,m} C_{lnm} \exp[-(\Lambda_0)_m T] \times \exp[-(\Lambda_{-1})_n(t_2 + b_2) - ia_2] \times \Im \sum_j B_{lj} \exp[-(\Lambda_j)(t_1 + b_1)]. \quad [12]$$

Note that in Eqs. [11] and [12] $B_{lj} \equiv B_{lj}^+$; i.e., the superscript has been omitted for convenience. In this case, the first step of the phase cycle measures the real part in t_1 , given by Eq.

[11]. The phase of the preparation pulse is then advanced by $\pi/2$ for the second half of the phase cycling to collect the imaginary part in t_1 , given by Eq. [12]. Equations [11] and [12] provide the dual-quadrature or hypercomplex data set, i.e., $\Re_2\Re_1$, $\Im_2\Re_1$, $\Re_2\Im_1$, and $\Im_2\Im_1$, where \Re and \Im stand for real and imaginary part of the signal and the subscripts refer to the two time axes. When b_1 , a_2 , and b_2 are nonzero, there will be an admixture of absorptive and dispersive components in the frequency-domain spectra, as discussed below, and this will require phase correction.

The phase errors are primarily due to two sources. The first is an imperfect bandwidth due to the finite irradiating fields and pulses. Gorcester and Freed (1) analyzed this using a classical vector model and they found that it led to a linear phase variation across the two-dimensional frequency spectrum.¹ Additionally, instrumental dead times (of about 50 ns in t_1 and 40 ns in t_2 in current work in our lab) contribute a further phase error given by $\Phi(\omega_0 - \omega_{rf}) = (\omega_0 - \omega_{rf})\tau_d/2\pi$ (1), where τ_d is the dead time.

However, most signals of interest in 2D ESR are strongly inhomogeneously broadened due to various reasons such as the presence of unresolved superhyperfine interactions, and the effects of MOMD [microscopic order but macroscopic disorder (cf. Results and Discussion)] and of very slow motions (3).

Common phase-correction techniques used in high-resolution 2D NMR (13) rely on separating out the real and imaginary parts of the t_1 data in the two parts of the phase cycle (cf. Eqs. [11] and [12]). However, this is strictly valid only for negligible inhomogeneous broadening. The presence of inhomogeneous broadening invalidates this in two ways. First, in the presence of inhomogeneous broadening, the t_1 -dependent terms in the collected signal (cf. Eq. [8] and Eq. [9]) are not pure real and imaginary, respectively. Second, after the dead time, the S_{c+} signal is much weaker than the S_{c-} signal (cf. Eq. [5]). In fact, in extreme (but frequent) cases, we lose the S_{c+} signal completely, and then $S' \propto S_{c-}$; $S'' \propto i \times S_{c-}$. Again this causes the t_1 -dependent terms to deviate from a simple real or imaginary behavior. The presence of these two factors ensures that we no longer have two independent complex functions to phase the spectra and hence commonly used 2D NMR procedures (13) are not immediately applicable.

Note that, in the fast motional regime, absorption spectra can also be obtained by other methods. For example, for fast motions and small inhomogeneous broadening, the model based on LPSVD (11, 24, 25) is valid and has been used to calculate the pure absorption spectra (2, 16).

Additionally in the slow-motional regime, however, the

¹ Note that the imperfect coverage would also lead to a frequency-dependent amplitude variation of the 2D ESR spectrum, and for quantitative analysis, this is also corrected (1, 2).

weighting factors C_{lm} and B_{lj} become complex, and the very concept of a pure absorption spectrum requires special care. To appreciate this, consider the single-pulse FID (3). The signal, S^{FID} , is given by

$$S^{\text{FID}}(t_2) = \sum_j C_j \exp[-(\Lambda_{-1})_j t_2] \quad [13]$$

$$C_j = \sum_{pk} (\nu_{-1})_p (O_{-1})_{pj} (O_{-1})_{kj} (\nu_{-1})_k. \quad [14]$$

A Fourier transform of this signal provides the CW equivalent spectrum,

$$S^{\text{FID}}(\omega_2) = \sum_j C_j (A_{2j} + iD_{2j}), \quad [15]$$

where A_{2j} and D_{2j} are the absorptive and dispersive contributions to the lineshape from each dynamic ‘‘spin packet.’’ They are defined as

$$A_{2j} \equiv A_{2j}(\omega_2) = T_{2j}^{-1} / [(T_{2j}^{-1})^2 + (\omega_2 - \omega_j)^2] \quad [16]$$

$$\begin{aligned} D_{2j} &\equiv D_{2j}(\omega_2) \\ &= (\omega_2 - \omega_j) / [(T_{2j}^{-1})^2 + (\omega_2 - \omega_j)^2]. \end{aligned} \quad [17]$$

Also, ω_2 is the Fourier transform frequency component corresponding to t_2 , and its zero refers to the center resonance frequency. The real and imaginary parts of the signal in Eq. [15] correspond to the standard absorption and dispersion spectra in CW ESR spectroscopy. These are given by

$$\text{Abs} \equiv \Re[S^{\text{FID}}(\omega_2)] = \sum_j \{\Re[C_j]A_{2j} - \Im[C_j]D_{2j}\} \quad [18]$$

$$\begin{aligned} \text{Dis} &\equiv \Im[S^{\text{FID}}(\omega_2)] \\ &= \sum_j \{\Re[C_j]D_{2j} + \Im[C_j]A_{2j}\}. \end{aligned} \quad [19]$$

Note that while D_{2j} appears in Eq. [18], it has always been found that slow-motional absorption CW ESR spectra are pure positive, as required for an absorption experiment. This suggests that the negative excursions due to the dispersive components are counterbalanced by larger absorptive components. However, these dispersive components contribute to the complexity of the slow-motional lineshape. We will take Eqs. [18] and [19] as operative definitions for absorption and dispersion for slow-motional ESR (and NMR).

In the next subsection it is shown that by suitable transformations and phase corrections we can calculate, for the COSY or SECSY experiment,

$$S_{c-}(\omega_1, \omega_2) = \sum_j A_{1j} [\Re(C_{jj})A_{2j} - \Im(C_{jj})D_{2j}]. \quad [20]$$

A comparison of Eqs. [20] and [18] shows that Eq. [20] has a form very similar with respect to ω_2 to that of the CW spectrum. In the ω_1 direction we obtain simple absorption lineshapes. This method is then extended to the 2D ELDOR case, and it is shown that, in the slow-motional regime, we can recover absorption-like lineshapes for the autopeaks in an ELDOR experiment. However, the cross peaks can be mixed mode in general. Finally in the subsection Phase Factors, we provide an approach for determining the relevant phase factors, based on nonlinear least-squares techniques.

Slow Motions with Large Inhomogeneous Broadening

SECSY and COSY. In the slow-motional regime, the weighting factors B and C are complex, as noted above. Further, the signals are usually strongly inhomogeneously broadened. Consequently, the S_{c+} signal typically decays away in the dead time. Therefore, the method of choice must be based on the ‘‘echo-like’’ S_{c-} signal. We now describe such a procedure for the SECSY experiment, where the echo is measured after a two-pulse sequence, and we show how a simple variant of this is applicable for the case of COSY.

The SECSY signal is given by

$$\begin{aligned} S_{c-}(t_1, t_2) &= \sum_{nj} K_{nj} \exp[-\{(\Lambda_{+1})_j + (\Lambda_{-1})_n\}(t_1 + b_1)] \\ &\times \exp[-(\Lambda_1)_n(t_2 + b_2) - ia_2] \exp[-\Delta t_2^2], \quad [21] \end{aligned}$$

where

$$K_{nj} = \sum_l C_{ln} B_{lj}^+. \quad [22]$$

The terms C_{ln} and B_{lj}^+ are given in Eqs. [3] and [4], respectively.

For the case of a COSY experiment, Lee *et al.* (3) demonstrated that the S_{c-} spectrum is symmetric about the $t_1 = t_2$ axis. In fact, it is this feature that gives rise to the echo. A shearing transform (3, 26) $t_2 \rightarrow t_1 + t_2$ recovers the equivalent of the SECSY experiment (i.e., substituting $t_2 \rightarrow t_1 + t_2$ in Eq. [2] for S_{c-} gives Eq. [21]). Physically, this arises because a SECSY experiment is essentially a time-shifted COSY experiment. Therefore, one first obtains the $S_{c-}(t_1, T, t_2)$ combination as given by Gamliel and Freed (23) for the COSY experiment. Upon performing the shearing transform the signal is identical to SECSY (cf. Eq. [21]) and hence the following discussion is applicable for both the SECSY and COSY experiments.

For these experiments a further simplification can be made. In the absence of nuclear modulation, the eigenvalues in the two off-diagonal spaces are complex conjugates of

each other (3). Also the autopeaks occur at $j = n$ and hence for the autopeaks the sum reduces to

$$\begin{aligned} S_{c-}^{\text{auto}}(t_1, t_2) &= \sum_j K_{jj} \exp[-\{\text{Re}(\Lambda_{-1})_j\}(t_1 + b_1)] \\ &\times \exp[-\{(\Lambda_1)_j(t_2 + b_2) + ia_2\}] \\ &\times \exp[-\Delta t_2^2]. \quad [23] \end{aligned}$$

In fact, we find from simulations that the SECSY experiment is dominated by the autopeaks, and so we shall take Eq. [23] to apply generally to a good approximation. Note that the argument of the exponential in t_1 is pure real, and so it will yield simple exponential decays. A Fourier transform of Eq. [23] with respect to t_2 gives

$$\begin{aligned} S_{c-}^{\text{auto}}(t_1, \omega_2) &= G(\omega_2) \\ &\otimes \sum_j K_{jj} \exp[-\{\text{Re}(\Lambda_{-1})_j\}(t_1 + b_1)] \\ &\times \exp[-i\phi_2](A_{2j} + iD_{2j}), \quad [24] \end{aligned}$$

where the symbol \otimes stands for the convolution integral, A_{2j} and D_{2j} are defined in Eqs. [16] and [17], respectively, and

$$G(\omega_2) = \sqrt{\frac{\pi}{\Delta}} \exp\left[-\frac{\omega_2^2}{\Delta}\right] \quad [25]$$

$$\phi_2 = \omega_2 b_2 + a_2. \quad [26]$$

The real and imaginary parts of Eq. [24] are given by

$$\begin{aligned} \Re[S_{c-}^{\text{auto}}(t_1, \omega_2)] &= G(\omega_2) \otimes \sum_j \exp[-\{\text{Re}(\Lambda_{-1})_j\}(t_1 + b_1)] \\ &\times [\{\Re(K_{jj})A_{2j} - \Im(K_{jj})D_{2j}\} \cos \phi_2 \\ &+ \{\Re(K_{jj})D_{2j} + \Im(K_{jj})A_{2j}\} \sin \phi_2] \quad [27] \end{aligned}$$

$$\begin{aligned} \Im[S_{c-}^{\text{auto}}(t_1, \omega_2)] &= G(\omega_2) \otimes \sum_j \exp[-\{\text{Re}(\Lambda_{-1})_j\}(t_1 + b_1)] \\ &\times [\{\Re(K_{jj})D_{2j} + \Im(K_{jj})A_{2j}\} \cos \phi_2 \\ &- \{\Re(K_{jj})A_{2j} - \Im(K_{jj})D_{2j}\} \sin \phi_2]. \quad [28] \end{aligned}$$

Comparing Eqs. [27] and [28] with Eqs. [18] and [19] allows us identify the absorption (A'_{2j}) and dispersion (D'_{2j}) lineshapes in ω_2 as

$$A'_{2j} \equiv \Re(K_{jj})A_{2j} - \Im(K_{jj})D_{2j} \quad [29]$$

$$D'_{2j} \equiv \Re(K_{jj})D_{2j} + \Im(K_{jj})A_{2j}. \quad [30]$$

With these definitions Eqs. [27] and [28] can then be rewritten as

$$\begin{aligned} & \Re[S_{c-}^{\text{auto}}(t_1, \omega_2)] \\ &= G(\omega_2) \otimes \sum_j \exp[-\{\text{Re}(\Lambda_{-1})_j\}(t_1 + b_1)] \\ & \quad \times [A'_{2j} \cos \phi_2 + D'_{2j} \sin \phi_2] \end{aligned} \quad [31]$$

$$\begin{aligned} & \Im[S_{c-}^{\text{auto}}(t_1, \omega_2)] \\ &= G(\omega_2) \otimes \sum_j \exp[-\{\text{Re}(\Lambda_{-1})_j\}(t_1 + b_1)] \\ & \quad \times [D'_{2j} \cos \phi_2 - A'_{2j} \sin \phi_2]. \end{aligned} \quad [32]$$

From Eq. [31] it is clear that the presence of phase variation leads to a mixture of absorption with some dispersion in the real part of the $S_{c-}^{\text{auto}}(t_1, \omega_2)$ signal. To rectify this, we can phase correct the signal as

$$\begin{aligned} S_{a-}^{\text{auto}}(t_1, \omega_2) &= \cos \phi_2 \Re[S_{c-}^{\text{auto}}(t_1, \omega_2)] \\ & \quad - \sin \phi_2 \Im[S_{c-}^{\text{auto}}(t_1, \omega_2)] \end{aligned} \quad [33]$$

to give

$$\begin{aligned} S_{a-}^{\text{auto}}(t_1, \omega_2) &= G(\omega_2) \\ & \quad \otimes \sum_j \exp[-\{\text{Re}(\Lambda_{-1})_j\}(t_1 + b_1)] A'_{2j}; \end{aligned} \quad [34]$$

i.e., we can recover absorption-like lineshapes (analogous to Eq. [18] for the single pulse FID) in ω_2 . Since the t_1 terms in Eq. [34] provide decaying exponentials only, we would expect $S_{a-}^{\text{auto}}(t_1, \omega_2)$ to be pure positive. On Fourier transforming Eq. [34] with respect to t_1 we get

$$\begin{aligned} S_{a-}^{\text{auto}}(\omega_1, \omega_2) &= G(\omega_2) \otimes \sum_j A'_{2j} \exp(-ib_1 \times \omega_1) \\ & \quad \times (A_{1j} + iD_{1j}). \end{aligned} \quad [35]$$

A_{1j} and D_{1j} are defined as

$$A_{1j} \equiv \frac{\Re(\Lambda_{-1})_j}{(\Re\Lambda_{-1})_j^2 + \omega_1^2} \quad [36]$$

$$D_{1j} \equiv \frac{\omega_1}{(\Re\Lambda_{-1})_j^2 + \omega_1^2}. \quad [37]$$

The frequency-domain spectrum can then be phase corrected in ω_1 in a manner similar to Eq. [33] to obtain the absorption spectrum,

$$\begin{aligned} S_{a-}^{\text{auto}}(\omega_1, \omega_2) &= \cos(b_1\omega_1) \Re[S_{a-}^{\text{auto}}(\omega_1, \omega_2)] \\ & \quad - \sin(b_1\omega_1) \Im[S_{a-}^{\text{auto}}(\omega_1, \omega_2)], \end{aligned} \quad [38]$$

which yields

$$S_{a-}^{\text{auto}}(\omega_1, \omega_2) = G(\omega_2) \otimes \sum_j A_{1j} A'_{2j}. \quad [39]$$

The lineshapes in ω_1 are of a simple absorption type (cf. Eqs. [36] and [39]), i.e., a sum of Lorentzians with simple homogeneous linewidths given by $\Re(\Lambda_{-1})_j$.

Therefore, for the COSY (and SECSY) experiment, use of the shearing transformation and phase correction and an application of the Fourier transform allow us to obtain absorption-like lineshapes in ω_2 and ω_1 .

2D ELDOR. The success of the above procedure in yielding absorption-like lineshapes for the two-pulse experiments encourages one to generalize the method to the three-pulse 2D ELDOR case. Therefore, we first apply the shearing transformation on the time-domain $S_{c-}(t_1, T, t_2)$ data (cf. Eq. [5]) which gives

$$\begin{aligned} & S_{c-}(t_1, T, t_2) \\ &= \sum_{nmj} K_{nmj} \exp[-\{(\Lambda_{+1})_j + (\Lambda_{-1})_n\}(t_1 + b_1)] \\ & \quad \times \exp[-(\Lambda_0)_m T] \exp[-(\Lambda_{-1})_n(t_2 + b_2) - ia_2] \\ & \quad \times \exp\{-\Delta t_2^2\}. \end{aligned} \quad [40]$$

Here

$$K_{nmj} = \sum_l C_{lmn} B_{lj}^+. \quad [41]$$

The weighting factors C_{lmn} and B_{lj}^+ are defined by Eqs. [6] and [7], respectively. In Eq. [40] the t_1 terms are clearly complex. Further, the T-dependent term consists of either pure exponential decaying functions or real oscillating sinusoids (22). After Fourier transforming Eq. [40] with respect to t_2 and phase correcting as defined Eq. [33], i.e.,

$$\begin{aligned} S_{a-}(t_1, T, \omega_2) &= \cos \phi_2 \Re[S_{c-}(t_1, T, \omega_2)] \\ & \quad - \sin \phi_2 \Im[S_{c-}(t_1, T, \omega_2)], \end{aligned} \quad [42]$$

we get

$$\begin{aligned} S_{a-}(t_1, T, \omega_2) &= G(\omega_2) \otimes \sum_{nmj} \exp[-(\Lambda_0)_m T] \end{aligned}$$

$$\begin{aligned} & \times (A'_{2n} \Re \exp[-\{(\Lambda_{+1})_j + (\Lambda_{-1})_n\}(t_1 + b_1)] \\ & + D'_{2n} \Im \exp[-\{(\Lambda_{+1})_j + (\Lambda_{-1})_n\}(t_1 + b_1)]). \end{aligned} \quad [43]$$

$G(\omega_2)$ is given in Eq. [25]. Also, A'_{2n} and D'_{2n} , the absorptive and dispersive components in ω_2 , are defined in a manner similar to Eqs. [18] and [19], i.e.,

$$A'_{2n} \equiv \Re(K_{nmj})A_{2n} - \Im(K_{nmj})D_{2n} \quad [44]$$

$$D'_{2n} \equiv \Re(K_{nmj})D_{2n} + \Im(K_{nmj})A_{2n}. \quad [45]$$

The autopeaks in 2D ELDOR occur at $j = n$. Since $\Lambda_{+1} = \Lambda_{-1}^*$, we have

$$\begin{aligned} & \Re \exp[-\{(\Lambda_{+1})_j + (\Lambda_{-1})_n\}(t_1 + b_1)] \\ & = \exp[-\Re(\Lambda_{-1})_j(t_1 + b_1)] \end{aligned} \quad [46]$$

$$\Im \exp[-\{(\Lambda_{+1})_j + (\Lambda_{-1})_n\}(t_1 + b_1)] = 0. \quad [47]$$

Hence, for autopeaks, Eq. [43] reduces to

$$\begin{aligned} \Re[S_{a^-}^{\text{auto}}(t_1, T, \omega_2)] & = G(\omega_2) \otimes \sum_{mj} \exp[-(\Lambda_0)_m T] A'_{2j} \\ & \times \exp[-\Re(\Lambda_{+1})_j(t_1 + b_1)]. \end{aligned} \quad [48]$$

On Fourier transforming Eq. [48] with respect to t_1 and phase correcting in a manner identical to Eq. [38], i.e.,

$$\begin{aligned} S_{a^-}(\omega_1, T, \omega_2) & = \cos(b_1\omega_1) \Re[S_{a^-}(\omega_1, T, \omega_2)] \\ & + \sin(b_1\omega_1) \Im[S_{a^-}(\omega_1, T, \omega_2)], \end{aligned} \quad [49]$$

we get for the autopeaks

$$\begin{aligned} S_{a^-}^{\text{auto}}(\omega_1, T, \omega_2) & = G(\omega_2) \otimes \sum_j \exp[-(\Lambda_0)_m T] A_{1j} A'_{2j}. \end{aligned} \quad [50]$$

A_{1j} has been defined in Eq. [36]. $S_{a^-}^{\text{auto}}(\omega_1, T, \omega_2)$ is similar to that for the SECSY experiment (Eq. [39]). Therefore, it is evident that absorption-like spectra can be obtained for the autopeaks in a 2D ELDOR experiment.

Examining Eq. [43] shows that the lineshapes of the cross peaks would be predicted to be mixed mode in general. However, as a practical matter a large number of theoretical simulations have shown that negative excursions in the cross peaks (expected due to the presence of dispersive components) are minimal for finite inhomogeneous broadening, Δ . It is there-

fore postulated that the presence of an inhomogeneous spread (which is less effectively canceled out for the cross peaks than the autopeaks) in frequencies causes these dispersive components to rapidly decay away in the dead time. Paradoxically, the presence of finite dead times are actually helpful in extracting pure absorption spectra. This is in accord with the experience of Grandinetti *et al.* (15) for time-shifted 2D dynamic-angle spinning NMR experiments. Again, they rationalized this behavior as due to the presence of a Lorentzian-type inhomogeneous broadening which caused the dispersive components to decay away rapidly in t_1 .

Phase Factors

The above prescriptions rely on accurate knowledge of the actual phase factors in the experiment. The general procedure for obtaining them would be to first phase the $t_1 = 0$ slice (which is unaffected by modulation in t_1) to obtain the ω_2 phase factors, and then the $t_1 = 0$ slice (constructed from the full two-dimensional data set) is phased for phase factors in ω_1 . However, due to finite dead times in both t_1 and t_2 , this method is not available in 2D FT ESR. One can of course phase up a single-pulse FID from the sample (with the same dead time in t_2 and coverage) to obtain phase factors in ω_2 but then those in ω_1 are undetermined.

We describe a method for circumventing this problem. One can obtain good "seed" values for a_2 , b_1 , and b_2 by modeling a fast-motional signal with well-characterized properties (e.g., PDT/toluene) collected under similar experimental conditions, using LPSVD (16). The actual phase factors for the sample of interest can be slightly different from these, since different samples and temperatures can slightly change the resonator quality factor, Q , as well as the operating frequency. This would change the coverage in the experiment and hence the phase factors. However, for a particular sample and temperature, they would be independent of mixing time.

If we examine Eq. [39] for the SECSY/COSY experiment in the light of Eq. [18], we can make the *ansatz* that the absorption spectrum is pure positive. This has been confirmed by us by many theoretical simulations. Therefore, after Fourier transforming with respect to t_2 , the seed values of the phase factors a_2 and b_2 required for phasing $S_{a^-}^{\text{auto}}(t_1, \omega_2)$ (cf. Eq. [33]) are (nonlinearly) optimized so as to minimize the function κ , defined as

$$\kappa = \left[\sum_{i,j}^{n_1, n_2} S_{i,j} \right]^2 \quad \forall S_{i,j} < 0, \quad [51]$$

where S_{ij} is the spectrum at the i th value of t_1 and the j th value of ω_2 , and n_1 and n_2 are the number of points in t_1 and ω_2 , respectively. Thus, minimization of κ corresponds to the minimization of the negative excursions in the (t_1 ,

ω_2) spectrum. Following phase correction in ω_2 , $S_{a-}(t_1, \omega_2)$ (cf. Eq. [34]) is Fourier transformed with respect to t_1 and the function κ is recalculated according to the equivalent of Eq. [51]. The phase factor b_1 required to properly phase $S_{a-}^{\text{auto}}(\omega_1, \omega_2)$ (cf. Eq. [38]) is again optimized by minimizing κ . Brent's algorithm, based on the principal-axis method (27), was used to optimize the phase factors. The penalty paid for this procedure is in the form of increased data processing. However, computationally the method is not demanding, so that the increased time is not very excessive. This method was successfully tested on theoretical simulations where a finite dead time was introduced to produce phase errors (cf. next section).

For the 2D ELDOR experiment, the above *ansatz* of a pure positive spectrum is correct only for the $T \approx 0$ experiment. This corresponds to the limit where a 2D ELDOR experiment is equivalent to a COSY. Cross peaks grow in with mixing time, and these, having a mixed-mode character (cf. Eq. [43]), would violate the condition of pure positivity. Therefore, one should phase correct the lowest mixing time experiment (i.e., $T \approx 0$) and use the phase factors obtained for the longer mixing times.

Comparison with Theory

For simulations, we assume that the pulses are perfectly nonselective (3). Hence, the only source of phase variations is the dead times in t_1 and t_2 . In fact, these are known exactly from Eq. [21], i.e.,

$$a_2 = 0 \quad [52]$$

$$b_2 = \tau_{2d} \quad [53]$$

$$b_1 = \tau_{1d}, \quad [54]$$

where τ_{1d} and τ_{2d} are the dead times in t_1 and t_2 , respectively. Hence the phase errors can be rectified directly in the time domain, so Eq. [21] becomes

$$S_{c-}(t_1, t_2) = \sum_{nj} K_{nj} \exp[-\{(\Lambda_{+1})_j + (\Lambda_{-1})_n\}t_1] \\ \times \exp[-(\Lambda_1)_n t_2] \exp\{-\Delta t_2^2\} \quad [55]$$

and the form for the autopeaks (cf. Eq. [23]) becomes

$$S_{c-}^{\text{auto}}(t_1, t_2) = \sum_j K_{jj} \exp[-\{\text{Re}(\Lambda_{-1})_j\}t_1] \\ \times \exp[-(\Lambda_1)_j t_2] \exp[-\Delta t_2^2]. \quad [56]$$

We Fourier transform Eq. [56] with respect to t_2 and extract the real part. This is then Fourier transformed in t_1 and the real part of the transform gives

$$\Re[S_{c-}^{\text{auto}}(\omega_1, \omega_2)] = G(\omega_2) \otimes \sum_j A'_{2j} A_{1j}, \quad [57]$$

where A'_{2j} and A_{1j} have been defined in Eqs. [29] and [36], respectively. Note that Eq. [57] corresponds to the phased experimental spectra given by Eq. [39], as it should. Hence we can make a direct comparison between theory and experiment. The approach for the case of 2D ELDOR is exactly the same, and it yields Eq. [50] for the autopeaks.

EXPERIMENTAL

Samples

CSL samples. A measured amount (0.346 ml) of 1.9 mM CSL in chloroform stock solution was added to 50 mg of POPC (in excess chloroform) to yield a 1 mol% concentration of the spin probe. The sample was contained in a 3 mm o.d. glass tube. The chloroform was removed by desiccating on the vacuum line for about 24 hours and a small excess of water was added to form a saturated dispersion. The sample was then degassed to a pressure of about 1×10^{-4} Torr and sealed.

Peptide samples. The peptide systems studied were (a) A P P P P C-MTSSL I (monoradical) and (b) MTSSL-C P P P P C-MTSSL II (biradical) where (i) MTSSL is the methanethiosulfonate spin label and (ii) A, C, and P are amino acids alanine, cysteine, and proline, respectively. These short-chain peptides were custom synthesized at the Cornell Biotechnology Department and were labeled with the MTSSL spin label via a disulfide bond (28). The MTSSL spin label was procured from Reanal (Budapest, Hungary). The concentrations of the two systems were about 1.5 mM. The sample was prepared by dissolving the required amount of the peptide in a glycerol/water/trifluoroethanol mixture which was buffered with MOPS [3-(*N*-morpholino)propanesulfonic acid] at pH 7, in a glove bag.

2D FTESR Experiments

All experiments were performed on the 2D FT ESR spectrometer, which has been described elsewhere (1). The use of a TWTA with an output power of 1–2 kW as well as a loop-gap resonator allowed uniform coverage of about ± 100 MHz. The pulse sequences used are shown in Fig. 1. COSY and 2D ELDOR experiments were performed on both samples. A 16-step phase cycle for COSY and a 32-step phase cycle for 2D ELDOR were used to eliminate all unwanted terms. These are based on the 8- and 16-pulse sequences given elsewhere (23). The additional steps in the phase cycle serve to further eliminate instrumental artifacts not fully removed by the original sequence (6). The nominal width of a $\pi/2$ pulse was 4.9 ns.

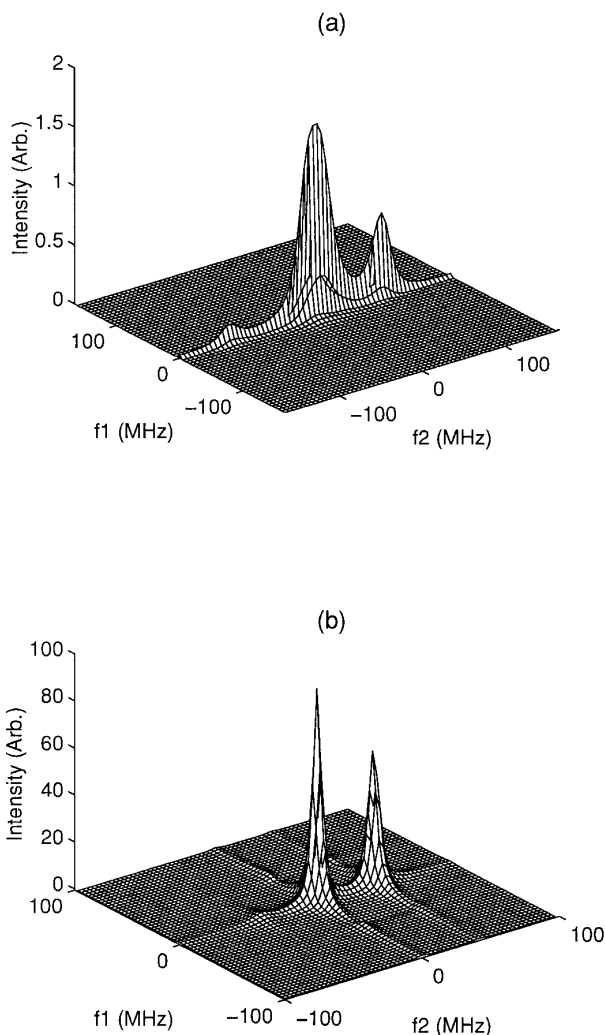


FIG. 2. Absorption spectra obtained from theoretical simulations for the SECSY experiment. (a) A typical very slow-motional spectrum. The parameters used are $R_{\perp} = 1.7 \times 10^5 \text{ s}^{-1}$, $R_{\parallel} = 1.7 \times 10^6 \text{ s}^{-1}$, and $\Delta_G = 2.0 \text{ G}$. (b) A typical MOMD spectrum obtained using 20 orientations. The parameters used are $R_{\perp} = 2.3 \times 10^8 \text{ s}^{-1}$, $R_{\parallel} = 2.3 \times 10^9 \text{ s}^{-1}$, $S = 0.08$, $\Delta_G = 0.5 \text{ G}$, and $\omega_{\text{HE}} = 1 \times 10^6 \text{ s}^{-1}$. The dead times in t_1 and t_2 for (a) and (b) were 40 ns each. Also, the magnetic parameters used are $g_{xx} = 2.0081$, $g_{yy} = 2.0061$, $g_{zz} = 2.0024$, $A_{xx} = 5.6$, $A_{yy} = 5.3$, and $A_{zz} = 33.8$.

CSL samples. We collected 256 points at a step size of 1 ns in t_2 after a dead time of 75 ns for ELDOR and 62 ns for COSY. The separation between the first two pulses, t_1 , was stepped with 128 steps of 3 ns from an initial value of 50 ns. The 2D ELDOR experiments were repeated for a series of mixing times, T , ranging from 74 ns to 3 μs . Results were obtained at several different temperatures.

Peptide samples. At the temperature range and motional rate studied, the T_2^* (≈ 5 to 10 ns) were too short to allow the detection of the free induction decay, but an echo decay can readily be measured. For the 2D ESR experiments, the

initial value of t_1 was 50 ns and 128 steps of 3 ns were collected. For each t_1 step, 256 data points at a 1 ns interval were measured in t_2 after a spectrometer dead time of 40 ns.

RESULTS AND DISCUSSION

We would first like to demonstrate that the absorption spectrum from a COSY/SECSY experiment is positive definite, using simulations. Two cases are of experimental interest: (a) very slow motion, where the spectrum is sensitive to the details of motional mechanisms, and (b) samples where the spectrum is a superposition of spectra from locally ordered environments (or fragments) which are randomly

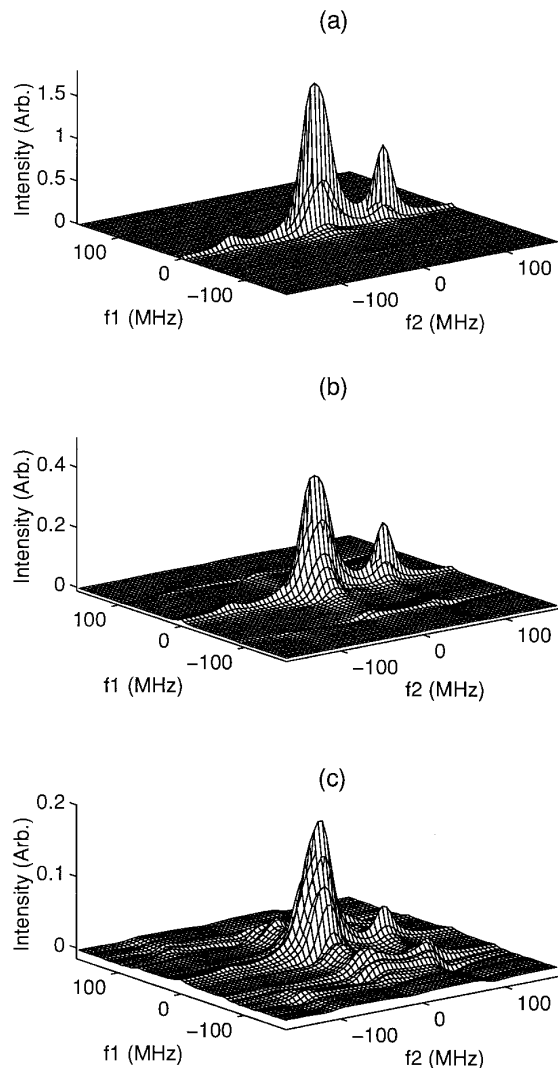


FIG. 3. Absorption spectra obtained from theoretical simulations for the 2D ELDOR experiment. Simulation parameters are the same as those in Fig. 2a. Spectra are shown for different mixing times, T : (a) 100 ns, (b) 1 μs , and (c) 5 μs .

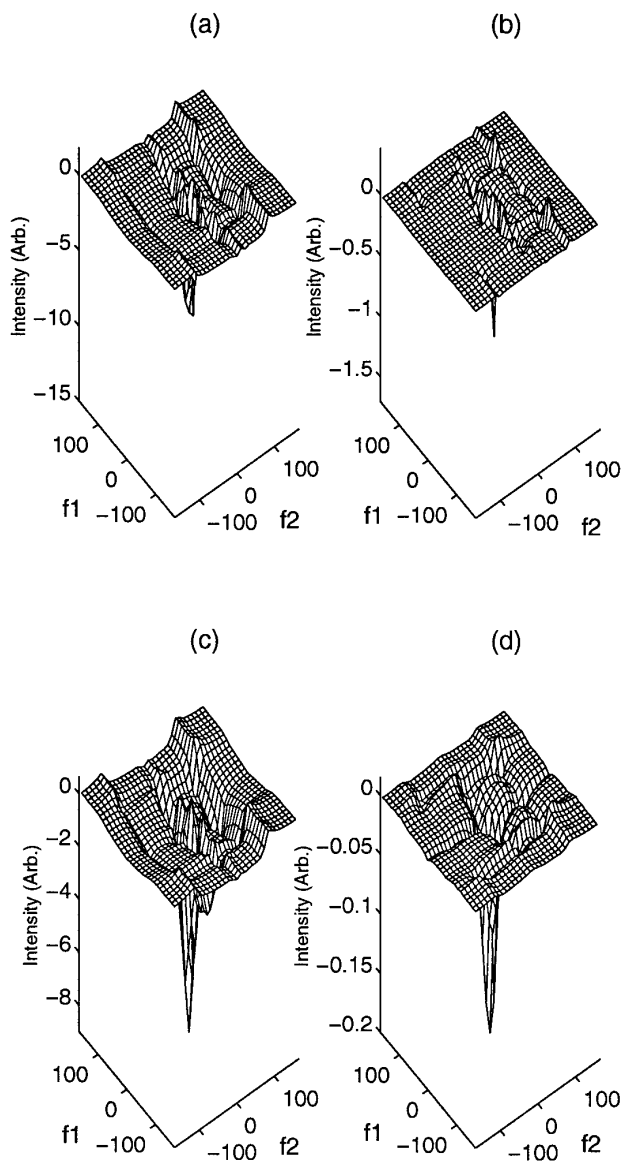


FIG. 4. Negative of 2D ELDOR absorption spectra, $T = 5 \mu\text{s}$. The simulation parameters are the same as those in Fig. 2a except for the inhomogeneous broadening parameter and the dead times: (a) $\Delta_G = 0.1$ G and dead times are 0 ns, (b) $\Delta_G = 0.1$ G and dead times are 40 ns, (c) $\Delta_G = 2.0$ G and dead times are 0 ns, and (d) $\Delta_G = 2.0$ G and dead times are 40 ns.

distributed; i.e., the sample is microscopically ordered but macroscopically disordered (referred to as MOMD) (3, 5, 6). The MOMD case is important for biologically relevant membrane systems, where it is not conveniently possible to prepare macroscopically aligned samples, although macroscopically disordered “dispersion” samples are readily available.

In Fig. 2 we show theoretical absorption spectra obtained using Eq. [55] for SECSY, for the cases (a) and (b). The parameters used to simulate these spectra are provided in

the legend. We find that the use of Eq. [57] for the autopeaks in SECSY gives virtually identical results to those from Eq. [55] in the cases tested. Hence, the spectra in Fig. 2 are found to be pure positive. As noted earlier, the COSY S_c -signal after the shearing transformation is formally equivalent to a SECSY signal. We have found that the *ansatz* of pure positivity of the SECSY spectrum is true for theoretical absorption spectra obtained for a large range of parameters. Hence, this criterion can be safely imposed while phasing SECSY/COSY experimental spectra using Eqs. [33], [38], and [51].

In Fig. 3, theoretical absorption spectra are shown for the 2D ELDOR case corresponding to the parameters of Fig. 2a. Here Eq. [40] is used with the phase corrections of Eqs.

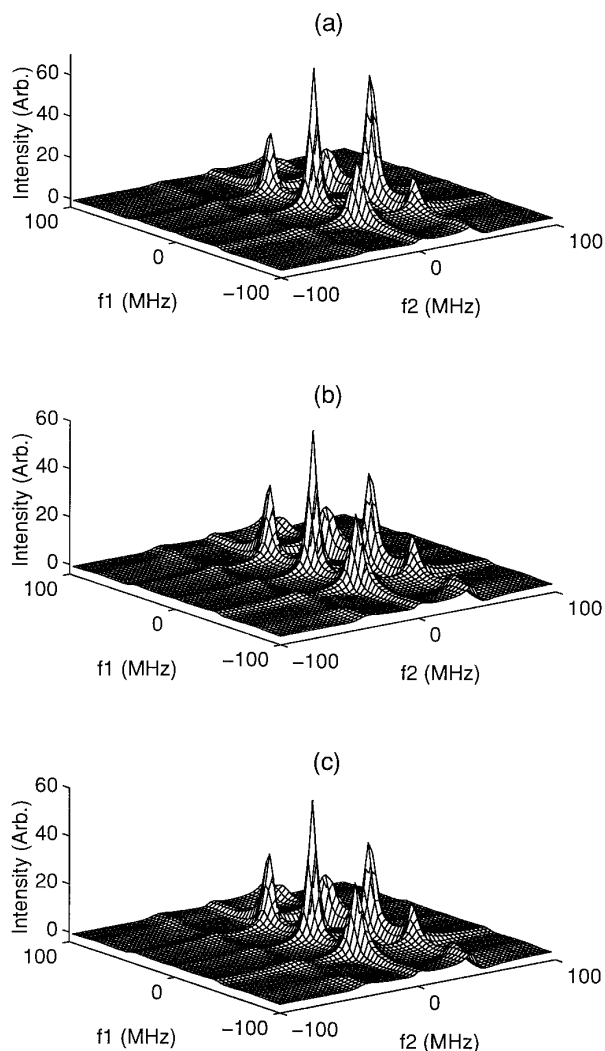


FIG. 5. Absorption spectra obtained from theoretical simulations for the 2D ELDOR experiment. Simulation parameters are the same as those in Fig. 2b. Spectra are shown for different mixing times, T : (a) 150 ns, (b) 1 μs , and (c) 3 μs .

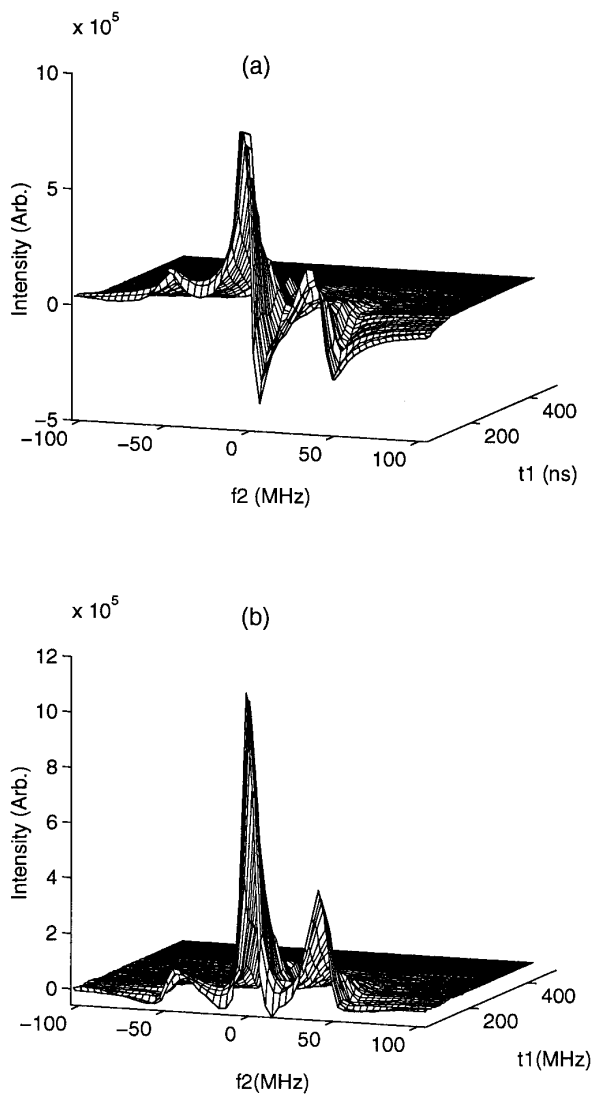


FIG. 6. Experimental COSY S_{c-} data from CSL/POPC at 70°C after the shearing transformation $t_2 \rightarrow t_2 + t_1$ shown in a (t_1, ω_2) format: (a) before phase correction and (b) after phase correction in ω_2 .

[52] – [54]. While absorption-like lineshapes are recovered for the autopeaks, small dispersive components in the cross peaks appear for larger mixing times (cf. Fig. 3c for $T = 5 \mu\text{s}$), leading to negative excursions in the 2D spectra. This is shown more clearly in Fig. 4 where the negative of the data is plotted, for $T = 5 \mu\text{s}$, at two different values of the inhomogeneous broadening parameter Δ_G (0.1 and 2.0 G) and dead times (0 and 40 ns) each. For zero dead times (cf. Figs. 4a and 4c), there are small dispersive components present which lead to negative (positive in the spectra shown) excursions. However, for finite dead times (cf. Figs. 4b and 4d), these components largely decay away in the dead times. For large dead times these features would be within the noise in the spectrum. Hence, we find that it is

safe to use a small mixing time 2D ELDOR spectrum to optimize the experimental phase factors as described in the subsection Phase Factors. These can then be used to phase correct the 2D ELDOR experimental spectra obtained for all the other mixing times, at that temperature.

Theoretical absorption spectra for the MOMD case are shown in Fig. 5. The contribution to the inhomogeneous broadening due the MOMD effect is important for this discussion (6). During the evolution period, t_1 , a spin label belonging to hyperfine (hf) component ‘a’ will evolve with an inhomogeneity associated with this hf component. After it exchanges to hf component ‘b’ during the mixing time, T (leading to a cross peak in the spectrum), it will evolve in t_2 with the refocused inhomogeneity associated with the component, b. Therefore, inhomogeneities associated with the MOMD effect, which are different for ‘a’ and ‘b’ (3)

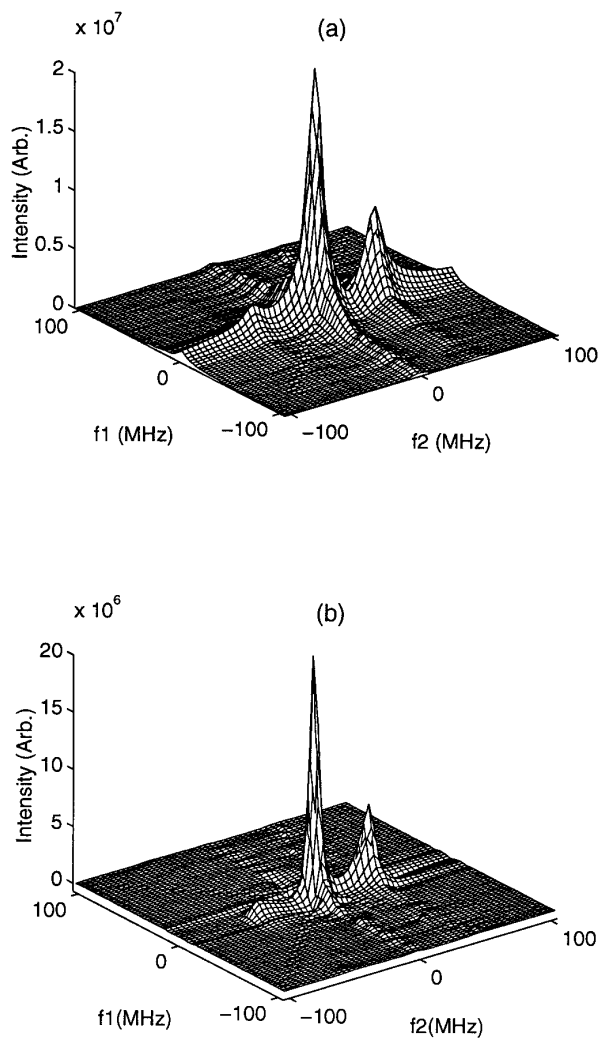


FIG. 7. Same data as Fig. 6 after the second Fourier transform. (a) Magnitude $S_{c-}(\omega_1, \omega_2)$ and (b) absorption.

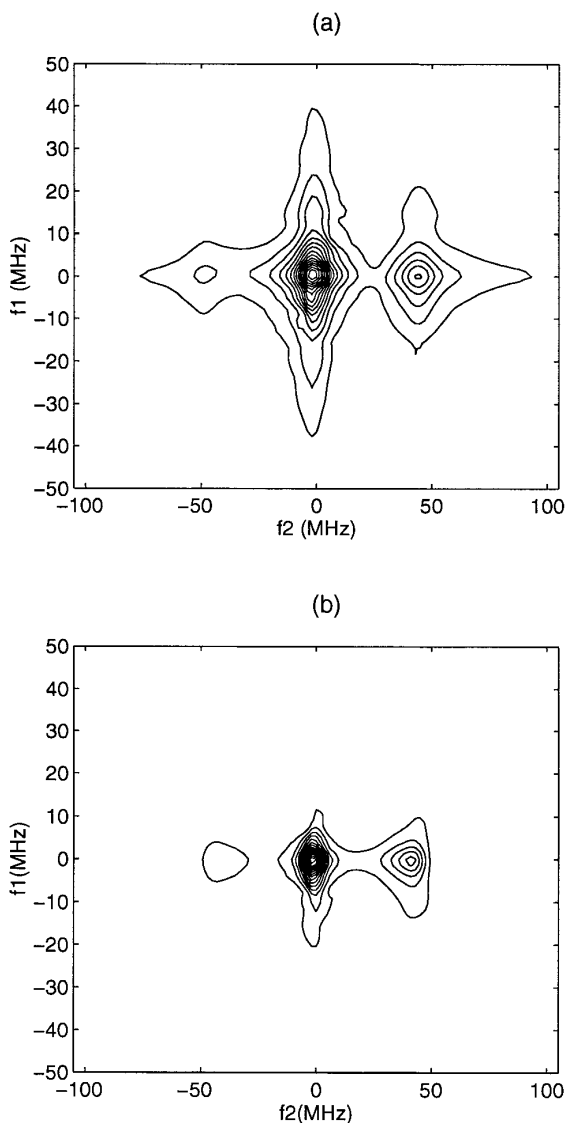


FIG. 8. Contour plots of spectra in Fig. 7 demonstrating the gain in resolution. (a) Magnitude and (b) absorption.

(as opposed to the proton superhyperfine interactions, where they are the same), will be less effectively refocused in the cross peaks. This extra broadening ensures that the dispersive components in the cross peaks are largely eliminated from the spectrum. Hence, the negative excursions of the cross peaks in Fig. 5 are relatively small. The *ansatz* of pure positivity for the 2D ELDOR spectrum from such MOMD-like samples is thus acceptable even for larger mixing times.

We now turn to some experimental results. The experimental methodology of obtaining the pure absorption spectrum is shown in Figs. 6 and 7 for a COSY experiment. In Fig. 6a a typical spectrum from an incipient slow-motional and highly ordered MOMD system (CSL/POPC at 70°C) is shown. The rotational mobility of the spin-labeled molecule,

CSL, is characterized by the rotational diffusion constants, R_{\perp} and R_{\parallel} , which represent the principal values of an axially symmetric rotation diffusion tensor. For CSL, these represent the motion perpendicular and parallel to the long molecular axis. The molecules in the bilayers experience ordering potentials, which can be characterized by an order parameter, S , defined as the first moment of the probability distribution in this potential (6). For this sample at this temperature the rotational rates were found to be $R_{\perp} = 8.5 \times 10^7 \text{ (s}^{-1}\text{)}$, $R_{\parallel} = 2.3 \times 10^8 \text{ (s}^{-1}\text{)}$, and ordering $S = 0.66$ (6). The COSY spectrum was transformed into the SECSY format and is shown in the real (t_1, ω_2) domain. The mixture of absorption with dispersion due to the phase variation across the spectrum is clear (as is expected from Eqs. [31]).

Figure 6b shows the same figure after phase correction in f_2 , using Eq. [33] and Eq. [51]. The dispersive components in ω_2 have largely been eliminated. A small amount of negative excursion occurs only in the smallest t_1 slice, and this could be due to contributions from dead time or effects due to phase interaction between pulses. Note that the t_1 domain consists of a sum of decaying exponentials, consistent with Eq. [39].

In Fig. 7 the same experimental COSY spectrum is shown after the second Fourier transform and phase correction using Eq. [38]. The contour plots are provided in Fig. 8. Both the

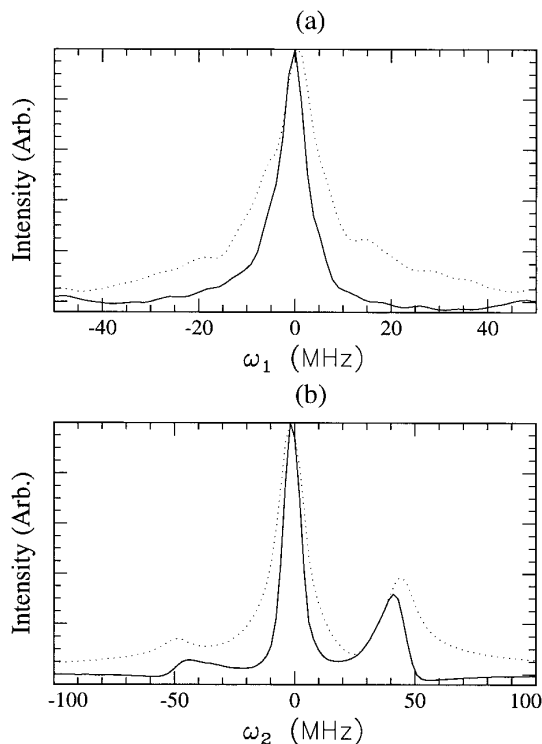


FIG. 9. Slices along a constant (a) ω_1 and (b) ω_2 for the spectra in Fig. 7. The absorption lineshape is the solid line while the magnitude spectra is the dotted line.

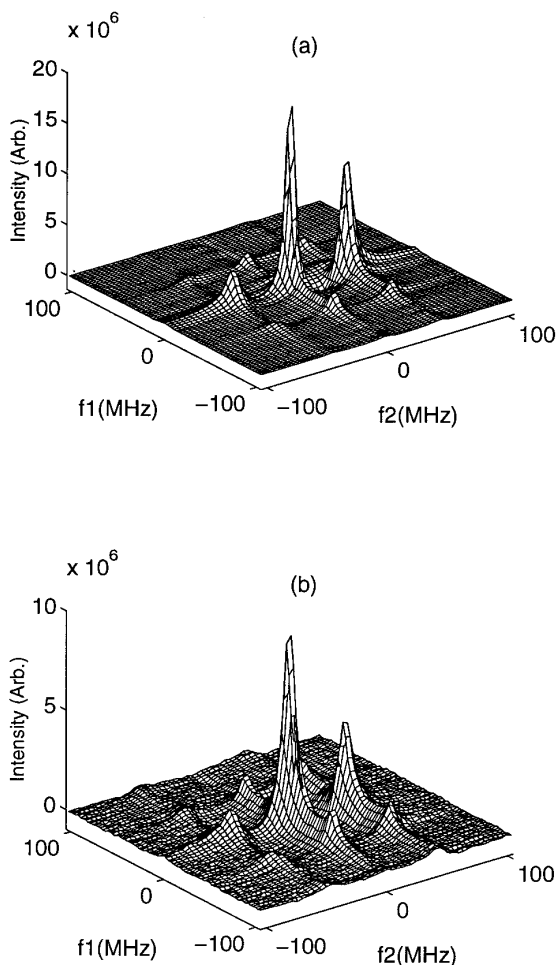


FIG. 10. Experimental 2D ELDOR spectra for CSL/POPC at 70°C. Absorption $S_{-}(\omega_1, \omega_2)$ at mixing times, T : (a) 166 ns and (b) 1 μ s.

magnitude and the absorption spectrum are shown in these figures. The gain in resolution is clear. For example, the linewidths are narrower in the pure absorption spectrum (cf. Fig. 8b) than in the magnitude-mode spectrum (cf. Fig. 8a). This is demonstrated more clearly in Fig. 9 where a single slice of data along ω_1 (cf. Fig. 9a) and along ω_2 (cf. Fig. 9b) is plotted for both the magnitude and the pure absorption spectrum shown in Fig. 7.

Figures 10 and 11 show the absorption (obtained by phase correction using Eqs. [42] and [49]) and magnitude spectra, respectively, for two ELDOR experiments at 70°C for CSL/POPC (corresponding to $T = 166$ ns and 1 μ s). The smaller mixing time (i.e., $T = 166$ ns) experiment was used to obtain the phase factors. Note that there is little evidence of dispersive peaks in the 2D double Fourier transform absorption spectra (cf. Fig. 10). This is reasonable for the CSL/POPC sample, as the 2D ELDOR spectra contain large contributions to the inhomogeneous broadening from the

MOMD effect. Also, the lines are sharper in the absorption mode and the peaks are better resolved. Such a gain in resolution is crucial for the accurate analysis of 2D ESR spectra in order to obtain reliable dynamic and ordering parameters (1, 2, 5, 6).

SECSY and 2D ELDOR absorption spectra for peptide I at -78°C are shown in absorption (Fig. 12) and magnitude (Fig. 13) modes. This corresponds to the case of very slow motions. Note that the sharpening of the spectrum is more dramatic in ω_1 than in ω_2 for the peptide sample (cf. Figs. 12 and 13). The likely reason for this is that spectra at this temperature are substantially broadened in ω_2 due to inhomogeneous contributions resulting from the slower motions. The pure absorption spectrum is not expected to remove this type of broadening. However, along ω_1 we obtain the natural linewidths [i.e., the homogeneous T_2 's (2, 3)]. The pure absorption widths are narrower as they remove the overlap effects inherent in the magnitude representation.

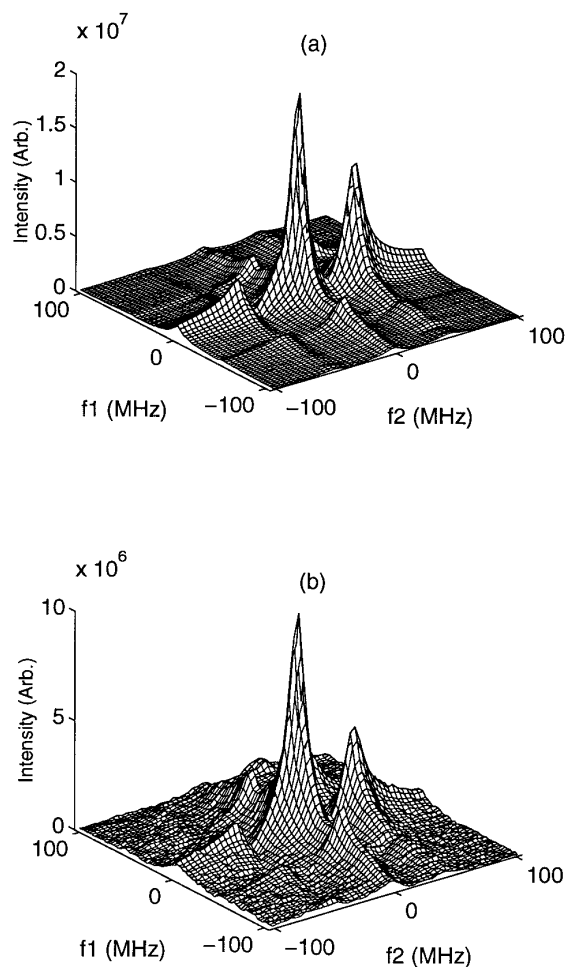


FIG. 11. Experimental 2D ELDOR spectra for CSL/POPC at 70°C. Magnitude $S_{-}(\omega_1, \omega_2)$ at mixing times, T : (a) 166 ns and (b) 1 μ s.

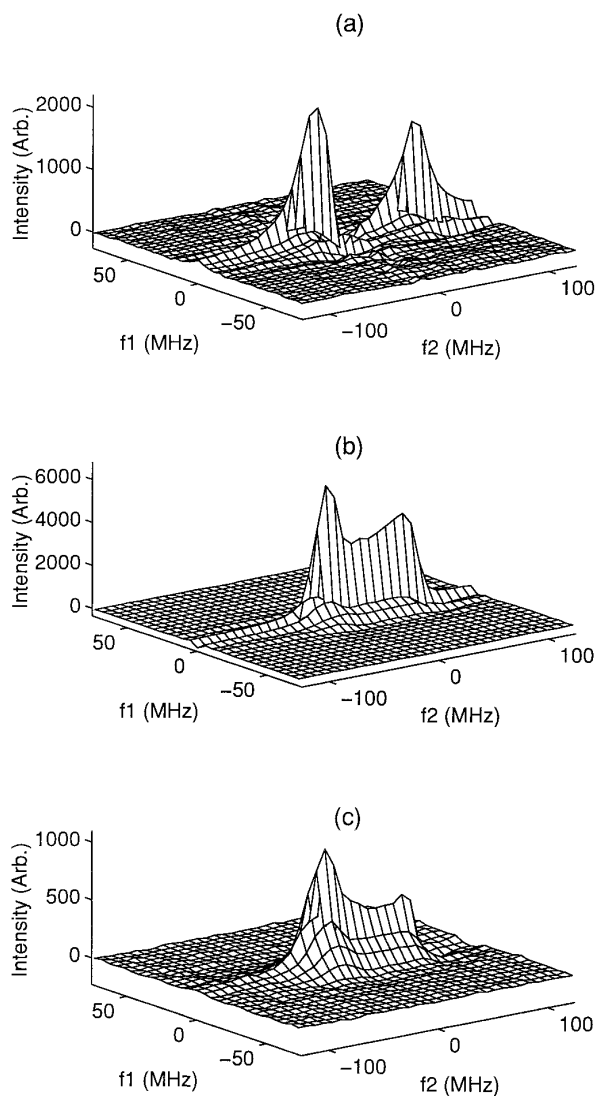


FIG. 12. Experimental 2D ESR spectra for peptide I at -78°C . Absorption $S_c(\omega_1, \omega_2)$ (a) SECSY and 2D ELDOR, (b) $T = 1 \mu\text{s}$, and (c) $T = 12 \mu\text{s}$.

We would now like to discuss the T_2 variation across the spectrum in a SECSY experiment. The clearest display of this is to plot the normalized contours of the spectrum. These are produced by dividing the $S(\omega_1, \omega_2)$ slice by the zero megahertz slice [i.e., $S(0, \omega_2)$]. Any variation of the homogeneous linewidth (i.e., T_2^{-1}) across the spectrum is immediately apparent. In Fig. 14 we show the normalized contours for peptide I in the absorption (Fig. 14a) and magnitude (Fig. 14b) modes. At -85°C the motion is largely quenched. This is reflected in the constant T_2 's in both the magnitude and absorption contours. However, at -50°C (where the sample is in the very slow-motional regime) the absorption contours (Fig. 14a) show a clear variation in T_2 's. This information is lost in the magnitude spectra (Fig. 14b).

In Fig. 15 we show the normalized contours for peptide II in the absorption (Fig. 15a) and magnitude (Fig. 15b) modes. This biradical had an interelectron distance of about 20 \AA (29, 30) which corresponds to a small dipolar interaction of about 2.3 G. The trend in the variation in T_2^{-1} is similar to that for the monoradical, as expected. However, the T_2 's are smaller (the normalized contours are further apart in Fig. 15 than in Fig. 14) than those of the monoradical, reflecting additional effects due to modulation of the small dipolar term.

SUMMARY

The presence of large inhomogeneous broadening in ESR makes commonly used 2D NMR (13) methods for obtaining

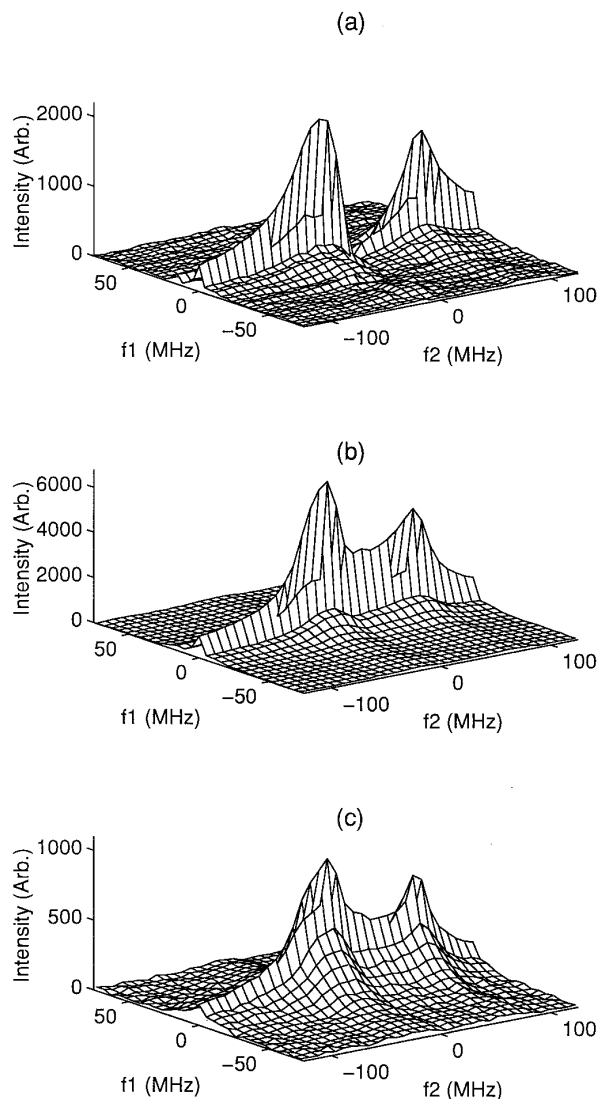


FIG. 13. Experimental 2D ESR spectra for peptide I at -78°C . Magnitude $S_c(\omega_1, \omega_2)$ (a) SECSY and 2D ELDOR, (b) $T = 1 \mu\text{s}$, and (c) $T = 12 \mu\text{s}$.

2D absorption spectra inapplicable. Further, the fact that slow-motional spectra consist of superimposed complex Lorentzians with complex weighting factors invalidates common assumptions of absorptive lineshapes which rely on the weighting factors being real. In such cases, it has usually been assumed that obtaining pure absorption 2D spectra in unachievable (19). We have extended the definition of absorption implicitly used for slow-motional 1D CW ESR spectra to two dimensions. The absorption spectra in 1D magnetic resonance are always positive (and hence absorption-like) despite the fact that, in the slow-motional regime, they contain “dispersive” contributions from each “dy-

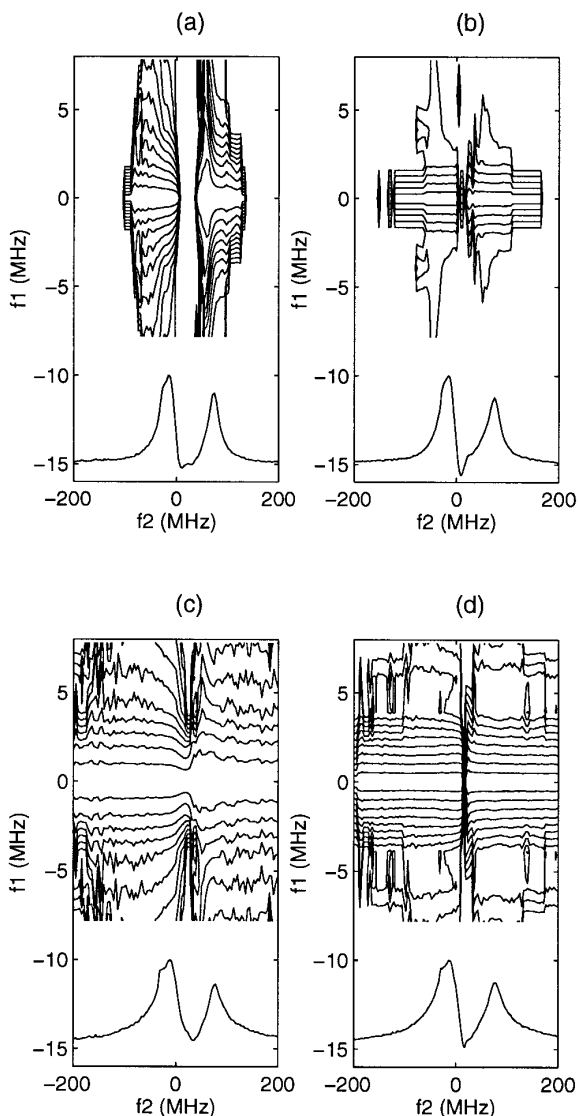


FIG. 14. COSY data for peptide I after the shearing transformation $t_2 \rightarrow t_2 + t_1$. Normalized contours are shown. Absorption contours at (a) -50°C and (b) -85°C and magnitude contours at (c) -50°C and (d) -85°C .

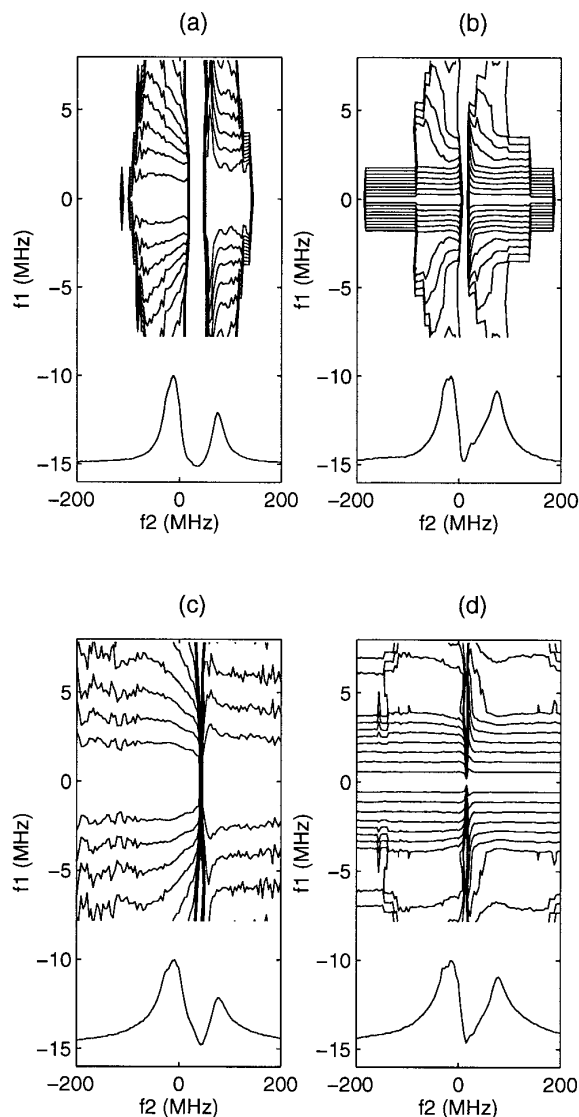


FIG. 15. COSY data for peptide II after the shearing transformation $t_2 \rightarrow t_2 + t_1$. Normalized contours are shown. Absorption contours at (a) -50°C and (b) -85°C and magnitude contours at (c) -50°C and (d) -85°C .

amic spin packet” according to basic theory. We have shown that such absorption-like spectra can be obtained for COSY and SECSY experiments.

Whereas phase corrections for the experimental data are necessary, these corrections are well defined for a given pulse spectrometer, although they vary slightly for different samples. Hence a procedure is provided for optimizing these phase corrections that is based on the *ansatz* of the pure positivity of COSY/SECSY spectra, which we have verified by simulations for a number of cases. Experimental absorption spectra obtained using this procedure are provided, and the enhanced resolution compared to the magnitude mode

is demonstrated. For example, the variation of the homogeneous linewidth across a SECSY spectrum is clearly rendered in the absorption mode, while it is obscured in the magnitude display. Further, lineshapes are narrower in the absorption mode than in the magnitude spectrum, providing increased spectral resolution.

The procedure is extended to the case of 2D ELDOR. It is shown that it is possible to obtain absorption-like lineshapes for the autopeaks, although the cross peaks can be of mixed-mode character, in general. However, simulated and experimental absorption spectra show that the dispersive components in the cross peaks would be small and relevant only for longer mixing times. Hence, phase corrections obtained from the shorter mixing time experiments can safely be used to correct the longer mixing time spectra.

Finally, we note that our definitions of absorption-like ESR spectra render the experimental data in a form where they can be directly compared to theory. This is essential for obtaining dynamic and ordering parameters which rely on making such comparisons.

ACKNOWLEDGMENTS

We thank Dr. J. Lin and Professor T. Thannhauser for the synthesis of the peptide samples. Helpful discussions with Professors D. E. Budil and S. Lee and Dr. R. H. Crepeau are also acknowledged. Computations were performed at the Cornell Theory Center and the Cornell Materials Science Center. This work was supported by the NIH under Grants RR07126 and GM25862 and by the NSF under Grant CHE 9313167.

REFERENCES

- (a) J. Gorcester and J. H. Freed, *J. Chem. Phys.* **85**, 5375 (1986);
(b) J. Gorcester and J. H. Freed, *J. Chem. Phys.* **88**, 4678 (1988).
- J. Gorcester, G. L. Millhauser, and J. H. Freed, in "Modern Pulsed and Continuous Wave Electron Spin Resonance" (L. Kevan and M. K. Bowman, Eds.), Wiley, New York, 1990.
- S. Lee, D. E. Budil, and J. H. Freed, *J. Chem. Phys.* **101**, 5529 (1994).
- J. H. Freed, G. V. Bruno, and C. F. Polnaszek, *J. Phys. Chem.* **75**, 3385 (1971).
- S. Lee, B. R. Patyal, S. Saxena, R. H. Crepeau, and J. H. Freed, *Chem. Phys. Lett.* **221**, 397 (1994).
- R. H. Crepeau, S. Saxena, S. Lee, B. R. Patyal, and J. H. Freed, *Biophys. J.* **66**, 1480 (1994).
- P. Bachmann, W. P. Aue, L. Muller, and R. R. Ernst, *J. Magn. Reson.* **28**, 29 (1977).
- G. Bodenhausen, R. Freeman, R. Niedermeyer, and D. L. Turner, *J. Magn. Reson.* **26**, 133 (1977).
- A. Bax, in "Two-Dimensional Nuclear Magnetic Resonance in Liquids," Kluwer Academic, Dordrecht/Norwell, Massachusetts, 1982.
- G. L. Millhauser and J. H. Freed, *J. Chem. Phys.* **81**, 37 (1984).
- G. L. Millhauser and J. H. Freed, *J. Chem. Phys.* **85**, 63 (1986).
- D. J. States, R. A. Haberkorn, and D. J. Ruben, *J. Magn. Reson.* **48**, 286 (1982).
- J. Keeler and D. Neuhaus, *J. Magn. Reson.* **63**, 454 (1985).
- A. Bax, A. F. Mehlkopf, and J. Smidt, *J. Magn. Reson.* **35**, 373 (1977).
- P. J. Grandinetti, J. H. Baltisberger, A. Llor, Y. K. Lee, U. Werner, M. A. Eastman, and A. Pines, *J. Magn. Reson. A* **103**, 72 (1993).
- J. Gorcester and J. H. Freed, *J. Magn. Reson.* **78**, 292 (1988).
- L. J. Schwartz, E. Meirovitch, J. A. Ripmeester, and J. H. Freed, *J. Phys. Chem.* **87**, 4453 (1983).
- D. Reimer, N. Heaton, A. Schleicher, K. Muller, G. Kothe, and M. Vilfan, *J. Chem. Phys.* **100**, 1693 (1994).
- K. Schmidt-Rohr and W. Spiess, in "Multidimensional Solid-State NMR and Polymers," Academic Press, San Diego, 1994.
- D. J. Schneider and J. H. Freed, in "Spin Labelling: Theory and Application" (L. J. Berliner and J. Reuben, Eds.), Plenum, New York, 1989.
- L. J. Schwartz, A. E. Stillman, and J. H. Freed, *J. Chem. Phys.* **77**, 5410 (1982).
- L. J. Schwartz, Ph.D. thesis, Cornell University, 1984.
- D. Gamliel and J. H. Freed, *J. Magn. Reson.* **89**, 60 (1990).
- R. Kumaresan and D. W. Tufts, *IEEE ASSP-30*, 833 (1982).
- H. Barkhuijsen, R. deBeer, W. M. M. J. Boveee, and D. Van Ormondt, *J. Magn. Reson.* **61**, 465 (1985).
- R. R. Ernst, G. Bodenhausen, and A. Wokaun, in "Principles of Nuclear Magnetic Resonance in One and Two Dimensions," Clarendon, Oxford, 1987.
- R. P. Brent, in "Algorithms for Minimization without Derivatives," Prentice-Hall, Englewood Cliffs, New Jersey, 1973.
- (a) S. M. Miick and G. L. Millhauser, *Biophys. J.* **63**, 917 (1992);
(b) Y. K. Shin, C. Levinthal, F. Levinthal, and W. L. Hubbell, *Science* **259**, 960 (1993).
- L. Stryer and R. Haugland, *Proc. Natl. Acad. Sci. USA* **58**, 719 (1967).
- S. Saxena and J. H. Freed, *Chem. Phys. Lett.* **251**, 102 (1996).